Spontaneous development of 3-D structure in sheared granular flows

James F. Lutsko*
Center for Nonlinear Phenomena and Complex Systems
Université Libre de Bruxelles
Campus Plaine, CP 231, 1050 Bruxelles, Belgium
(Dated: February 2, 2008)

Computer simulations of sheared granular fluids, modeled as inelastic hard spheres, are presented which show signs of a uniquely three-dimensional instabilty. In the stable regime, a linear velocity profile, $v_x = ay$, with shear rate a is established using Lees-Edwards boundary conditions. In the unstable regime, the velocity profile aquires a dependence on the third dimension of the form $v_x = ay + sin(2\pi z/L)$ in a cubic box with sides of length L. An analysis of the linearized Navier-Stokes equations shows the presence of an instability and gives a simple expression for the critical wavevector which is quantitatively consistent with the results of simulations and which indicates that the instability persists at low densities.

One of the intriguing aspects of fluidized granular flows is that they exhibit a rich phenomenology of clustering, segregation and pattern formation under different flow conditions(see e.g. [1],[2],[3]). Understanding the mechanisms that give rise to this behavior is one of the principle challenges in the field of granular physics. The minimal microscopic model of a granular fluid as hard spheres which lose energy upon collision is enough to give rise to many effects mentioned above. For example, computer simulations using this model of an isolated fluid shows that it is subject to both linear instabilities, which drive the formation of vortices[4],[5],[6], and nonlinear instabilities which lead to the formation of clusters[7],[8]. Similar phenomena are observed in both simulation and experiment of the more practically relevant sheared granular flows, in which the flow speed varies in some direction perpendicular to the direction of flow. Most attention has been focussed on 2-D flows due to the relative computational efficiency with which they can be simulated and ease with which they can be studied in experiments and the results visualized although a few experiments have probed the 3-dimensional structure in annular geometries[9]. It has long been known that 2-D flows show the formation of both large scale structures (shear bands) and small-scale ordering of the grains[10]. The analysis of the stability of shear flow is complicated by the convective terms which give rise to a coupling of hydrodynamic modes[11] for wavevectors that sample the direction of the flow but it has been shown that 2-D unbounded shear flows are linearly stable though subject to nonlinear instabilities that drive the pattern formation[10]. Bounded 2-D shear flows, with moving walls perpendicular to the velocity gradient and periodic boundaries in the direction of the flow, have been shown to be linearly unstable[12],[13]. Dense granular flows in 3 dimensions show solid-like ordering into regular arrays[9] reminiscent of that seen in elastic sheared fluids[14],[15].

In this work, I present the results of computer simulations of the minimal granular model subject to shear flow in an unbounded geometry using Lees-Edwards boundary conditions and show that the system develops 3-dimensional structure even at *low* densities where there is no sign of the solid-like ordering. In particular, the system develops an intermittant variation of the peculiar velocity (relative to the linear profile) as a function of position in the direction perpendicular to both the flow and the velocity gradient with clustering near the extrema of this profile. A linear stability analysis of the relevant hydrodynamic equations shows the presence of a linear instability towards perturbations with wavevectors in the third dimension and a simple stability criterion is derived. Interestingly, this instability appears to be very similar to one which occurs in the stability analysis of the HCS[16],[17],[6] but which is hidden by the nonlinear instabilities[8]. Based on these results it appears that 3-D sheared granular flows are linearly unstable for all densities.

The simulations described here of mechanically identical atoms were performed using an event-driven algorithm in which atoms stream freely between collisions. Two atoms with positions and velocities $\overrightarrow{q}_i, \overrightarrow{v}_i$ and $\overrightarrow{q}_j, \overrightarrow{v}_j$ collide when their separation $q_{ij} \equiv |\overrightarrow{q}_i - \overrightarrow{q}_j| = \sigma$ where σ is the hard-sphere diameter. The relative velocity $\overrightarrow{v}'_{ij}$ after the collision is related to that before the collision by

$$\overrightarrow{v}'_{ij} = \overrightarrow{v}_{ij} - (1 + \alpha)\,\widehat{q}_{ij}\widehat{q}_{ij} \cdot \overrightarrow{v}_{ij} \qquad (1)$$

where $\widehat{q}_{ij} = \overrightarrow{q}_{ij}/q_{ij}$ is a unit vector and the total momentum is unchanged. The parameter α is the coefficient of (normal) restitution: elastic hard spheres correspond to $\alpha = 1$ while for smaller values of α, energy is lost and the collisions are inelastic. More complex models allow for velocity-dependent coefficients of restitution and non-conservation of energy related to the tangential velocities as well but the focus here is on demonstrating the phenomena in the simplest model. The simulations
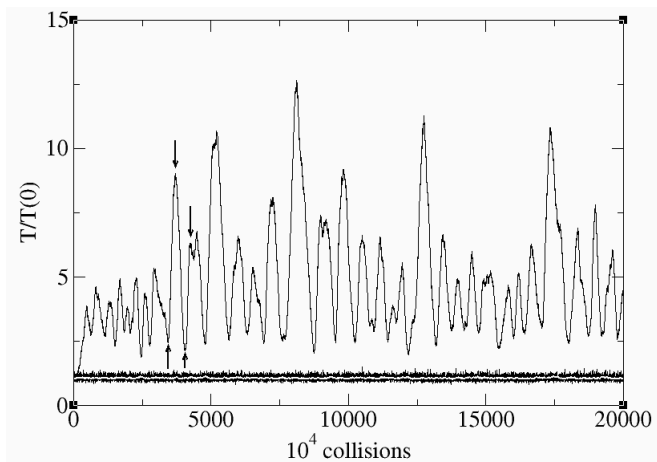
FIG. 1: Temperature as a function of the number of collisions for $\alpha = 0.7$ with 13500 grains, upper black line, 500 grains, lower black line, and $\alpha = 0.9, N = 13500$. white line. The arrows mark the times at which snapshots were taken. The arrows, from left to right, mark the snapshots (a)-(d) of the other figures.
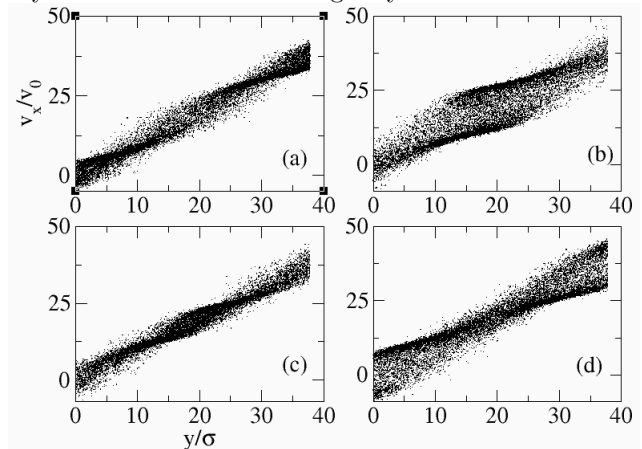

FIG. 2: Snapshots of the flow velocity as a function of position along the y axis. The velocities are scaled to the initial thermal velocity. Each point is one of the 13500 grains.

were performed in a cubic cell with walls of length L using Lees-Edwards boundary conditions[18] which are periodic boundaries in the Lagrangian frame defined by the velocity field $\vec{v}\left(\vec{r}\right) = ay\hat{x}$, where a is the shear rate. It is easy to show that the balance laws admit of a stationary, spatially homogeneous state with the collisional cooling balancing the viscous heating to give a constant temperature. This balance relates the temperature, applied shear rate and coefficient of restitution so that there are effectively only three independent dimensionless parameters which will here be taken to be the number of atoms, N, the size of the cell, L/σ, and the coefficient of restitution α. The temperature can always be set to $k_B T = 1$ by adjusting the time scale and the shear rate is then fixed by the energy balance relation. The procedure in all simulations was to first equilibrate an equilibrium ($\alpha = 1$ and so $a = 0$) liquid of the desired number of atoms and cell size by starting with a face-centered cubic configuration and allowing it to melt over a run of 5×10^7 collisions. Long before the end of these simulations, the system exhibits the expected pressure and diffusion constant of a hard sphere liquid. The shear rate and coefficient of restitution are then set to the desired values and the simulations continued.

A simple global measure of the behavior of the system is provided by the temperature defined as the kinetic energy calculated relative to the assumed linear shearing profile. Figure 1 shows the temperature as a function of time for $\alpha = 0.7$. The temperature of a small system, made up of 500 grains, is constant whereas that of the larger system, containing 13500 grains, increases rapidly and then appears to oscillate. The large deviation from between the two is an indication that the assumed profile

may be incorrect for the larger system. When α is set to 0.9, the larger system also appears to be stable. Figure 2 shows a snapshot of the velocity in the $x-$direction as a function of position in the y-direction for systems over one cycle of temperature oscillation while Fig. 2 shows the peculiar velocity $v_x - ay$ as a function of z for the same snapshots. The v_x vs y plot shows a generally linear profile but with clear signs of local structure which is presumably a manifestation of the kind of 2-D structure described previously[10]. The plot vs. z shows a clear sinusoidal variation with a time-varying amplitude that grows to many times the thermal velocity at its maximum. From the density of points in the figure, it is clear that there is some clustering at the positions of the maxima and minima of the curves. The snapshots taken at the minimum of the temperature cycle show that the 2-D structure persists but that the 3-D structure is virtually absent. Examination of numerous snapshots confirms that this oscillatory behavior takes place throughout the duration of the simulation and is the source of the temperature oscillations. As would be expected from Fig. 1, which shows that the temperature profiles for a small system of 500 grains at $\alpha = 0.7$ and and a 13500 grain system with $\alpha = 0.9$ are flat, neither of these systems exhibits this structure. Simulations of the larger system for $\alpha = 0.6$ show temperature variations that are more than 5 times greater than those for $\alpha = 0.7$.

To understand why some of the simulations would spontaneously develop the 3-D structure, it is natural to examine the linear stability of the system. The local hydrodynamic fields, the density $n\left(\vec{r}, t\right)$, temperature $T\left(\vec{r}, t\right)$ and the velocity $\overrightarrow{U}\left(\vec{r}, t\right)$, satisfy the exact balance equations[19],[20]
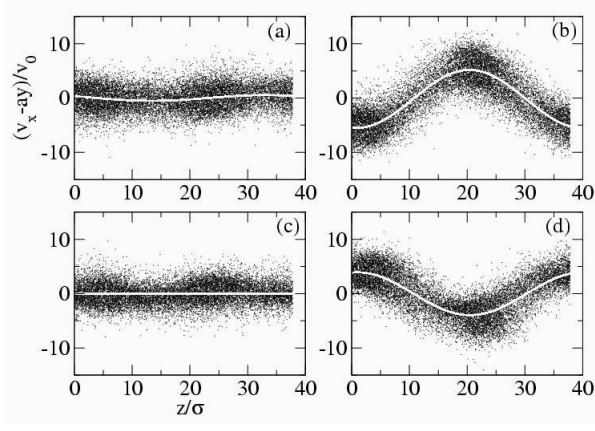
FIG. 3: Snapshots of the peculiar velocity in the x-direction as a function of position along the z axis. The velocities are scaled to the initial thermal velocity. Each point is one of the 13500 grains. The white line is a fit to a sin-function with wavevector fixed at $2\pi/L$.

$$
\frac{\partial}{\partial t}n + \overrightarrow{\nabla} \cdot \overrightarrow{U} n = 0 \tag{2}
$$

$$
\frac{\partial}{\partial t}T + \overrightarrow{U} \cdot \overrightarrow{\nabla} T + \frac{2}{Dnk_B}\overleftrightarrow{P} : \overrightarrow{\nabla}\overrightarrow{U} + \frac{2}{Dnk_B}\overrightarrow{\nabla} \cdot \overrightarrow{Q} = -\xi
$$

$$
\frac{\partial}{\partial t}\overrightarrow{U} + \overrightarrow{U} \cdot \overrightarrow{\nabla}\overrightarrow{U} + \frac{1}{mn}\overrightarrow{\nabla} \cdot \overleftrightarrow{P} = 0
$$

where $\overleftrightarrow{P}$ is the pressure tensor, $\overrightarrow{Q}$ is the heat flux vector and $\xi < 0$ is the cooling rate. Introducing the peculiar velocity $\overrightarrow{u}(\overrightarrow{r},t) = \overrightarrow{U}(\overrightarrow{r},t) - \overleftrightarrow{a} \cdot \overrightarrow{r}$ and using the

fluxes and cooling rate derived from the Enskog equation by expanding about HCS[19]

$$
P_{ij} = p\delta_{ij} - \eta(a_{ij} + a_{ji}) - \eta\left(\partial_i u_j + \partial_j u_i - \frac{2}{3}\delta_{ij}\overrightarrow{\nabla} \cdot \overrightarrow{u}\right) - \gamma\delta_{ij}\overrightarrow{\nabla} \cdot \overrightarrow{u} \tag{3}
$$

$$
Q_i = -\mu\partial_i n - \kappa\partial_i T
$$

$$
\xi = \xi^{(0)} + \xi^{(1)}\overrightarrow{\nabla} \cdot \overrightarrow{u}
$$

where p is the pressure, η is the shear viscosity, γ is the bulk viscosity, κ is the thermal conductivity and μ is a transport coefficient which goes to zero at $\alpha = 1$ and describes the fact that density gradients drive heat flow in the granular system. All of these quantities are functions of the local hydrodynamic fields. Expanding these fields about steady,uniform values as $n(\overrightarrow{r},t) = n_0 + \epsilon n_1(\overrightarrow{r},t) + ...$, where ϵ is a fictitious small parameter used to order a perturbative expansion of Eqs.(2-3), one finds at order ϵ^0 that the only nontrivial constraint

is the energy balance equation

$$
\eta_0 a^2 = \frac{3n_0}{2}\xi_0 \tag{4}
$$

where η_0 is the shear viscosity evaluated for the zeroth-order fields. This gives the constraint relating the shear rate to the cooling rate, and hence to the temperature and the coefficient of restitution. Note that this uniform solution is consistent with the periodic boundary conditions in the co-moving frame used in the simulations. Further details of the calculation, which is straightforward, will be given elsewhere and here, only the main

steps and results summarized. At linear order, it is convenient to switch to a Fourier representation but the stability analysis remains nontrivial due to the linear mode-coupling which occurs via the gradient term arising from the convective terms in eq.(3). However, to investigate stability in the $z-$direction, we can begin by restricting attention to wavevectors in that direction $\vec{k} = k\hat{z}$ in which case, several simplifications occur. First, the gradient term does not contribute, so that temporal stability is simply determined by the signs of the eigenvalues of the propagation matrix, the elements of which are quadratic functions of the wavevector. Second, the $x-$ and $y-$ components of the velocity. representing shear modes, decouple form the other variables and are purely decaying with time constant equal to the kinematic shear viscosity

is $\nu_0 = \frac{1}{mn_0}\eta_0$. The remaining three eigenvalues are the roots of a cubic secular equation with k-dependant coefficients. Setting $k = 0$ shows that two modes go to zero and the third is stable with a finite decay constant. The latter assures that small, homogeneous violations of the energy balance relation eq.(4) decay. The stability of the modes can be determined by looking for solutions of the secular equation for which the real part of the eigenvalue, λ, is zero, or in other words $\lambda = i\xi$ for real ξ. Then, the secular equation splits into two equations, the real and imaginary terms, which serve to determine both ξ and the critical wavevector k_c for which the mode does not decay. As expected, there are three possible solutions. In the first, $\xi = 0$ and the critical wavevector k_c satisfies

$$\left[\frac{\xi_n^{(0)}}{\xi_0^{(0)}} - \frac{\nu_n}{\nu} - \frac{p_n}{p_T}\left(\frac{\xi_T^{(0)}}{\xi_0^{(0)}} - \frac{\nu_T}{\nu}\right)\right]\frac{3n_0}{2}\xi_0^{(0)} = \left(\frac{p_n}{p_T}\kappa_0 - \mu_0\right)k_c^2 \tag{5}$$

where the shear rate has been eliminated using the energy balance equation. Here, a non-numerical subscript indicates a derivative evaluated in the homogenous state, e.g. $\nu_n = \left(\frac{\partial}{\partial n}\nu\right)_{n=n_0}$. Recall that μ_0 vanishes for $\alpha = 1$ so, for small deviations from elastic hard spheres, the coefficient on the right will be positive and, since $\xi_0^{(0)} > 0$, the critical wavevector exists if and only if the term in brackets is positive. It is easy to show by differentiating the secular equation that the slope of the real part of the eigenvalue at the critical wavevector is positive so that the mode is unstable for wavevectors smaller than the critical wavevector. The remaining two possibilities for critical wavevectors correspond to complex-conjugate propagating modes which become unstable but they are only relevant at extremely small values of α and will not be considered further here. Evaluation of this expression for the parameters of the simulation using the transport coefficients of ref.[19] gives $k_c\sigma = 0.238$. The instability will not be present for small systems since the smallest nonzero wavevector that can be sampled is $2\pi/L$ so that this defines a maximum stable system size or minimum number of grains in a given geometry. For a cubic system, this gives a stability limit of $N_c = 4612$ which is indeed between the sizes of systems examined here. Similarly, for fixed $N = 13500$, the instability exists for $\alpha < 0.804$ which is in agreement with the observations above. These calculations also show that the left hand side is positive for all α at zero density. Nevertheless, this calculation cannot be taken too seriously as the dependence of the transport properties on the shear rate has not been taken into account, although it might be hoped that the various ratios appearing in eq.(5) would be less sensitive to

this omission than the absolute values of the quantities.

The expression for the critical wavevector given in eq.(5) is closely related to a similar instability that occurs in the hydrodynamic equations linearized about the HCS[16],[17],[8]. Obviously, in the HCS there is no viscous heating to counteract the cooling of the gas, so the system is not in a steady state and hydrodynamic modes in the usual sense do not exist. However, the system can be mapped to a steady state by introducing a new time variable related nonlinearly to the laboratory time. This introduces source terms into the hydrodynamic equations which replace the two terms in eq.(5) involving the shear viscosity but the analysis is otherwise identical. As discussed in detail by Brey et al[8], this linear instability is not seen in the HCS because it is always slower to develop than the shear instability. The shear instability does not exist in sheared granular fluids and so it appears that the secondary instability identified in HCS is actually manifested.

These results only give information about the stability of the uniform velocity profile. Once the instability begins to develop, the nonlinear couplings in the hydrodynamic equations will become important and will govern the long time behavior. (Burnett terms and other higher order contributions to the fluxes neglected here will also become important.) In the present case, it is not clear whether these might exert a stabilizing influence that counteracts the linear instability, or whether the oscillations are due to a frustration of the system by the cubic simulation cell and periodic boundaries. A careful analysis of the effect of the nonlinear terms following along the lines of those performed for HCS[21],[8]

is clearly needed.

Very recently, simulations of 3-D shear flows have shown the presence of density variations along the third dimension (perpendicular to both the flow and the velocity gradient)[22].The simulations were performed using hard walls at $y = \pm L/2$ which move in the $\pm x$-direction thus creating a varying flow velocity between them and are characterized by the several collision parameters specifying the normal and tangential coefficients of restitution (governing the amount of energy and angular momentum lost in the collisions), for both the atom-atom and atom-wall collisions and are also complicated by the inevitable presence of boundary layers near the walls. It seems likely that this is a manifestation of the same phenomena.

---

* Electronic address: jlutsko@ulb.ac.be
[1] C. S. Campbell, Ann. Rev. Fluid Mechanics **22**, 57 (1990).
[2] H. M. Jaeger, S. R. Nagel, and R. P. Behringer, Phys. Today **49**, 32 (1996).
[3] H. M. Jaeger, S. R. Nagel, and R. P. Behringer, Rev. Mod. Phys. **68**, 1259 (1996).
[4] S. McNamara and W. R. Young, Phys. Rev. E **53**, 5089 (1996).
[5] J. A. G. Orza, R. Brito, T. P. C. van Noije, and M. H. Ernst, Int. J. Mod. Phys. C **8**, 953 (1997).
[6] J. J. Brey, J. W. Dufty, C. S. Kim, and A. Santos, Phys. Rev. E **58**, 4638 (1998).
[7] I. Goldhirsch and G. Zanetti, Phys. Rev. Lett. **70**, 1619 (1993).
[8] J. J. Brey, M. J. Ruiz-Montero, and D. Cubero, Phys. Rev. E **60**, 3150 (1999).
[9] J.-C. Tsai, G. A. Voth, and J. P. Gollub, Phys. Rev. Lett. **91**, 064301 (2003).
[10] M.-L. Tan and I. Goldhirsch, Phys. Fluids **9**, 856 (1997).
[11] J. Lutsko and J. W. Dufty, Phys. Rev. A **32**, 3040 (1985).
[12] M. Sasvari, J. Kertesz, and D. E. Wolf, Phys. Rev. E **62**, 3817 (2000).
[13] M. Alam and P. R. Nott, J. Fluid Mechanics **343**, 267 (1997).
[14] J. Erpenbeck, Phys. Rev. Lett. **52**, 1333 (1984).
[15] J. F. Lutsko, Phys. Rev. Lett. **77**, 2225 (1996).
[16] P. Deltour and J. L. Barrat, J. Phys. I **7**, 137 (1997).
[17] R. Brito and M. H. Ernst, Europhys. Lett. **43**, 497 (1998).
[18] A. Lees and S. Edwards, J. Phys. C **5**, 1921 (1972).
[19] V. Garzo and J. W. Dufty, Phys. Rev. E **59**, 5895 (1999).
[20] J. F. Lutsko, J. Chem. Phys. **to appear**.
[21] R. Soto, M. Mareschal, and M. M. Mansour, Phys. Rev. E **62**, 3836 (2000).
[22] S. L. Conway and B. J. Glasser, Phys. Fluids **16**, 509 (2004).